

^{19}F and ^{31}P magic-angle spinning nuclear magnetic resonance of antimony(III)-doped fluorapatite phosphors: Dopant sites and spin diffusion

Liam B. Moran

Michigan State University, Department of Chemistry, East Lansing, Michigan 48824-1322

Jeffery K. Berkowitz

GTE Electrical Products Corporation, 100 Endicott Street, Danvers, Massachusetts 01923

James P. Yesinowski*

Michigan State University, Department of Chemistry, East Lansing, Michigan 48824-1322

(Received 3 September 1991; revised manuscript received 20 November 1991)

Phosphors based on calcium fluorapatite [$\text{Ca}_5\text{F}(\text{PO}_4)_3$] doped with small amounts of Sb^{3+} as an activator are used in most fluorescent lamps. We have used quantitative ^{19}F and ^{31}P magic-angle spinning nuclear magnetic resonance (MAS-NMR) to study seven samples of calcium fluorapatite containing 0.0–3.0 wt % Sb^{3+} in order to determine the site of antimony substitution. The ^{31}P MAS-NMR spectra of fluorapatite containing 3.0, 2.1, and 1.3 wt % antimony contain a single sharp peak at 2.8 ppm indistinguishable from undoped fluorapatite, and show no additional peaks attributable to the influence of antimony. The ^{31}P MAS-NMR spectra of the model compounds SbPO_4 , $\text{Sr}_{1.03}\text{Ca}_{8.97}\text{F}_2(\text{PO}_4)_6$, $\text{Sr}_3\text{F}(\text{PO}_4)_3$, and $\text{Ba}_5\text{F}(\text{PO}_4)_3$ were also obtained. The ^{19}F MAS-NMR spectra of the antimony-doped samples exhibit, in addition to the main peak at 64.0 ppm (downfield from C_6F_6) arising from unperturbed fluorapatite, a shoulder at 65.6 ppm, and a sharp peak at 68.6 ppm. The measured spin-lattice relaxation times T_1 of these antimony-related peaks are equal in all cases to that of the main peak in a given sample, and vary from 129 to 378 sec, indicating that these peaks arise from apatitic fluoride ions perturbed by antimony. Quantitative studies reveal that the 68.6-ppm peak arises from two fluoride ions and the 65.6-ppm shoulder from one fluoride ion per Sb^{3+} ion incorporated into the lattice. The selective population anti- z and rate of transfer to adjacent nuclei (SPARTAN) pulse sequence used to measure spin diffusion by selectively inverting the 68.6-ppm peak reveals the presence of cross-relaxation to the main peak at 64.0 ppm, but not to the shoulder at 65.6 ppm. Each Sb^{3+} ion thus appears to be perturbing fluoride ions in at least two different chains. An additional peak at 73.1 ppm observed in some samples is assigned to a second type of antimony(III) substitution, with a single fluoride ion perturbed by each antimony ion. The results in total provide detailed support for a substitution model in which antimony(III) occupies a phosphate site in the apatite lattice, with a SbO_3^{3-} group replacing a PO_4^{3-} group. Two types of substitution at this site appear to occur, depending upon which oxygen atom is replaced by the antimony lone electron pair.

I. INTRODUCTION

The apatite structure,¹ with its extensive and varied substitutional chemistry,² is the basis for a wide variety of inorganic solids important in biomineralization, geology, and materials science. From the materials science standpoint, one extremely important technological application of apatites is as halophosphate phosphors in fluorescent lamps. The most commonly used phosphor is based on calcium fluorapatite [$\text{Ca}_5\text{F}(\text{PO}_4)_3$]. In commercial phosphors approximately 20% of the fluoride ions are replaced by chloride ions. Also, 0.5–1.0 wt % Sb^{3+} is present as an activator to absorb uv irradiation produced by the Hg discharge present in the lamp. The antimony subsequently converts this excitation energy into visible light by either of two processes. Direct Stokes-shifted emission from antimony can occur, or the excitation energy can be transferred to Mn^{2+} , present in 0.0–0.5 wt % quantities, which also emits light in the visible region of the spectrum. A detailed understanding of uv absorp-

tion, energy transfer, visible emission, and defect structures that lead to photodegradation requires knowledge of the lattice-substitution site of the activator ion. Whereas the substitutional sites and oxidation state for manganese have been well established,^{3,4} this is not true for antimony. Mössbauer results on antimony-doped calcium fluorapatite phosphors⁵ have shown that the antimony in the lattice has an oxidation state of +3. However, identification of the substitution site in the lattice is controversial, with at least two different sites having been proposed.^{5–9}

The fluorapatite structure features linear chains of crystallographically equivalent fluoride ions parallel to the c axis and extending the length of the crystal (Fig. 1).^{1,2} There are two types of calcium ions in the structure, labeled Ca(1) and Ca(2), in the ratio of 4:6. Surrounding each fluoride ion is an equilateral triangle of crystallographically equivalent Ca(2) ions that lie in a plane perpendicular to the fluoride chain. Adjacent triangles are rotated by 60° about the chain axis, creating a

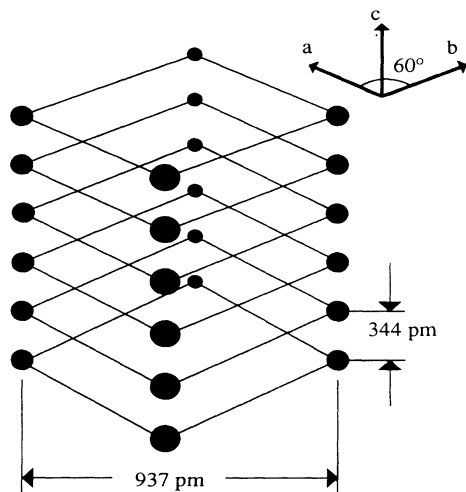


FIG. 1. Schematic diagram of the arrangement of four linear columns of fluoride ions (●) in the fluorapatite $[\text{Ca}_5\text{F}(\text{PO}_4)_3]$ lattice.

hexagonal screw axis in the structure. Adjacent to these Ca(2) sites are crystallographically equivalent phosphate tetrahedra. Finally, there are columns of Ca(1) ions running parallel to the c axis, each calcium column in the middle of an equilateral triangular prism formed by three fluoride columns.

Previous studies have considered three different possible substitution sites for antimony in the fluorapatite lattice. The first site of antimony substitution that has been considered is the Ca(1) site;⁵⁻⁷ however, no direct experimental evidence for this model has been found. A second model, based on Rietveld analysis of x-ray-powder-diffraction data, invokes the replacement of Ca^{2+} at the Ca(2) site with an Sb^{3+} ion;⁸ however, charge compensation was not explicitly discussed. Studies based on analyses of stoichiometry as well as spectroscopic data also support the replacement of Ca^{2+} at the Ca(2) site by Sb^{3+} , accompanied by the replacement of the adjacent fluoride ion by O^{2-} to achieve charge compensation.^{6,7,9} The third, most recent, model involves the substitution of phosphorus(V) in the phosphate tetrahedron by Sb^{3+} , with the loss of one oxygen atom of the tetrahedron providing charge compensation [the 5s electron lone pair of the antimony(III) atom is directed toward the missing oxygen-atom site in this model]. This phosphate-substitution model is based on measurements from Mössbauer data as well as theoretical calculations of antimony nuclear electric quadrupole-coupling constants.⁵

The determination of which of these conflicting proposals is correct, and whether there is exclusively one dopant-substitution site, requires a technique sensitive to local environments. High-resolution solid-state NMR, using the technique of magic-angle spinning (MAS),¹⁰ is widely used to determine local structure, but has rarely been applied to the study of dopants. The major difficulty in studying dopant atoms at low concentrations in solids is limited sensitivity. Most spin- $\frac{1}{2}$ nuclei have relatively low magnetogyric ratios and/or low natural abundances, and quadrupolar nuclei ($I > \frac{1}{2}$) usually exhibit excessive NMR spectral line broadening. However,

both ^{19}F , ^{31}P , and ^1H nuclei have natural abundances of 100% and large magnetogyric ratios, making them good prospects for studying dopants (the high-resolution ^{31}P and ^{19}F MAS-NMR spectra of undoped fluorapatite have already been reported¹¹⁻¹³). The large chemical-shift range of ^{19}F (several hundred ppm in metal fluorides¹⁴) makes it a particularly attractive probe nucleus. However, strong homonuclear dipolar couplings can make it difficult to obtain high-resolution MAS-NMR spectra, particularly for ^{19}F and ^1H , unless more involved multiple-pulse techniques are used.^{13,15} Fortunately, the availability of MAS rotor designs having high maximum spinning speeds, combined with the selection of samples having special structural arrangements, has made it possible to obtain high-resolution ^1H and ^{19}F MAS-NMR spectra in a variety of interesting systems. The special structural arrangements of homonuclear spins required include relatively isolated spin pairs,^{16,17} dilute spins, and linear chains of spins.¹⁸ The latter arrangement is characteristic of the fluorine atoms in fluorapatite, and high-resolution ^{19}F MAS-NMR spectra have been reported for calcium fluorapatite and fluorohydroxyapatites.¹²

The use of MAS-NMR to probe local structure has generally involved the measurement and interpretation of isotropic chemical shifts and possibly chemical-shift anisotropies. Special techniques to measure heteronuclear dipolar couplings have also proven useful.¹⁹⁻²¹ Homonuclear dipolar couplings of abundant spins in MAS-NMR spectra manifest themselves in (at least) two ways: as "dipolar sidebands" in the spectra^{16,17} and as the source of "spin-diffusion" contact among spins. Despite the great potential for obtaining local structural information from such spin-diffusion measurements, since the dipolar coupling is inversely related to the cube of the internuclear distance, few applications have been reported.²²⁻²⁵ In this study we demonstrate that in an abundant homonuclear dipolar system spectral spin diffusion between peaks with different isotropic chemical shifts can be observed using a one-dimensional (1D) MAS-NMR experiment referred to as selective population anti- z and rate of transfer to adjacent nuclei (SPARTAN).²⁶ A rotor-synchronized delays alternating with nutations for tailored excitation (DANTE) pulse train is used to invert selectively the magnetization of a ^{19}F peak and its associated sidebands, and all peaks are nonselectively observed after a mixing period during which spin diffusion occurs. The change in intensity of a peak resulting from cross-relaxation to other peaks as a function of mixing time provides a quantitative measure of spin diffusion and can aid in assignment of peaks.

In this study we report quantitative ^{19}F and ^{31}P MAS-NMR results for calcium fluorapatite samples containing 0.0-3.0 total wt % Sb^{3+} as well as ^{31}P MAS-NMR results for the model compounds SbPO_4 , $\text{Sr}_{1.03}\text{Ca}_{8.97}\text{F}_2(\text{PO}_4)_6$, $\text{Sr}_5\text{F}(\text{PO}_4)_3$, and $\text{Ba}_5\text{F}(\text{PO}_4)_3$. The ^{19}F and ^{31}P MAS-NMR results, including the ^{19}F MAS-NMR spin-diffusion experiments, will be discussed in relation to three possible models for substitution of antimony into the fluorapatite lattice. We will show that only the phosphate-substitution site (the third model) is consistent with the totality of experimental results.

II. EXPERIMENT

A. Sample preparation and characterization

The samples of antimony-doped fluorapatite that were prepared contained 0.00, 0.18, 1.3, 1.7, 2.1, and 3.0 wt % antimony(III) (determined by permanganate titration). Samples containing 0.00, 1.7, and 3.0 wt % antimony were prepared by combining $\text{Ca}_2\text{P}_2\text{O}_7$, CaO , CaF_2 , and CaSb_2O_6 (GTE Chemical and Metals Division, Towanda, PA) and firing in a covered Coors porcelain crucible at 1200°C . Both the 1.7 and 3.0 wt % antimony samples were firings of identical raw material blends. The difference in the final antimony levels in these two samples arises from significant vapor transport taking place during firing, as described in Ref. 8. Because of this vapor-transport process, it is difficult to control the final antimony level in a given sample. The samples containing 1.3 and 2.1 wt % antimony were prepared from identical raw material blends, but in a different manner than the samples containing 1.7 and 3.0 wt % antimony. The reagents CaHPO_4 , CaCO_3 , and CaF_2 (GTE Chemical and Metals Division, Towanda, PA) were first fired in stagnant air to create a fluorohydroxyapatite (with an indication of some carbonate substitution for phosphate from ir spectroscopy). CaSb_2O_6 and a small amount of $\text{Ca}_2\text{P}_2\text{O}_7$ were then fired with the precursor at 1200°C in a covered Coors porcelain boat. The 0.18-wt % sample was prepared by firing a combination of $\text{Ca}_2\text{P}_2\text{O}_7$, CaO , CaF_2 , and Sb_2O_3 at 1100°C in an open quartz boat with a flowing nitrogen atmosphere. Finally, the 0.8-wt % sample was a commercial halophosphate phosphor (GTE type 2440).

The specific surface areas of the samples containing 0.0 and 2.1 wt % antimony were measured using a Quantachrome Monosorb Brunauer-Emmett-Teller (BET) apparatus and were determined to be 0.626 ± 0.007 and 0.506 ± 0.004 m^2/g , respectively.

The SbPO_4 sample was obtained from GTE Chemical and Metals Division, Towanda, PA, and was annealed in air at 600°C for $\frac{1}{2}$ h to improve its crystallinity. Its identity was confirmed using x-ray powder diffraction (two small peaks attributable to Sb_2O_4 cervantite, were also present).

The $\text{Sr}_{1.03}\text{Ca}_{8.97}\text{F}_2(\text{PO}_4)_6$ sample was prepared by combining the following starting materials in the molar ratio: 6.0 mol CaHPO_4 , 2.982 mol CaCO_3 , 0.994 mol SrF_2 , and firing for 2 h at 1150°C under nitrogen in a Crystar crucible.

B. NMR equipment and procedures

The ^{31}P and ^{19}F MAS-NMR spectra were recorded on a 9.4-T Varian Associates VXR-400 spectrometer at the Max T. Rogers NMR Facility at Michigan State University, operating at frequencies of 161.76 and 376.2 MHz, respectively. The fluorine radio frequency was amplified by an AMT model 3137/3900-2 amplifier. The phosphorus radio frequency was amplified by an Amplifier Research model 1000LPM10 amplifier. A fast switching *p-i-n* diode was used to isolate the receiver during the pulse and $1.0 \mu\text{s}$ after the end of the pulse. The ^{19}F spectra were collected using an ultrahigh-speed ^{19}F MAS-

NMR probe from Doty Scientific (Columbia, SC) with 5-mm-o.d. Si_3N_4 rotors with Vespel caps. The probe was equipped with a fiber-optic detector to measure both the speed and position of the rotor for the rotor-synchronized spin-diffusion experiments. The 5-mm rotors contained approximately 160 mg of the sample, and spinning speeds ν_r were typically 8.25 ± 0.1 kHz. The $\pi/2$ pulses for ^{19}F were $4.0\text{--}4.2 \mu\text{s}$. The magic angle of the ^{19}F MAS-NMR probe was set by minimizing the linewidth of the fluorapatite peak. Chemical shift referencing of the ^{19}F MAS-NMR spectra was accomplished using fluorapatite prepared as in Ref. 12 as a secondary chemical-shift reference at 64.0 ppm (downfield) with respect to hexafluorobenzene at 0.0 ppm.¹² The ^{19}F MAS-NMR spectra were obtained with a 100-kHz spectral width, using 32 000 data points. An exponential weighting corresponding to a line broadening of 37 Hz (0.1 ppm) was applied to the free-induction decay (FID) before Fourier transformation. Eight transients were collected for each Bloch decay ^{19}F MAS-NMR spectrum with relaxation delays of at least 5 times the spin-lattice relaxation time T_1 .

The ^{31}P MAS-NMR spectra were obtained using a high-speed multinuclear MAS-NMR probe from Doty Scientific (Columbia, SC) with 7-mm-o.d. Si_3N_4 rotors with Vespel caps. The rotors contained approximately 500 mg of the sample. The probe was equipped with a fiber-optic detector to measure the spinning speed of the rotor. Spinning speeds ν_r for the ^{31}P MAS-NMR experiments were 6.15 ± 0.1 kHz, and the $\pi/2$ pulses were $6 \mu\text{s}$. The magic angle was set using the ^{79}Br resonance in KBr. The chemical shifts of the ^{31}P MAS-NMR spectra were measured using the peak of fluorapatite at 2.8 ppm downfield (with respect to 85% H_3PO_4) as a secondary chemical-shift reference.¹¹ The ^{31}P MAS spectra were obtained with a 30-kHz spectral width, using 48 000 data points. An exponential apodization was applied to the FID corresponding to a line broadening of 100 Hz.

The ^{31}P MAS-NMR spectra were obtained by collecting 80 transients using $\pi/4$ ($3\text{-}\mu\text{s}$) pulses and a delay time of 180 s between scans. Since ^{31}P MAS-NMR spin-lattice relaxation times can be extremely long in rigid solids (hours), the spectrum of the 2.1 wt % Sb^{3+} fluorapatite sample was also obtained using a very long relaxation delay of 3600 s and eight transients; no additional peaks due to a slowly relaxing component could be detected.

Values of the ^{19}F spin-lattice relaxation time T_1 were obtained using an inversion-recovery pulse sequence with four transients for each value of the delay time and a relaxation delay at least 5 times the T_1 of each sample. Thirteen delay-time values were used for each T_1 experiment. The T_1 values of the center bands and sidebands (equal within experimental error for a given sideband family) were calculated using peak heights and VNMR 2.2 software. Values of the ^{19}F transverse relaxation times T_2 were obtained using a rotor-synchronized Hahn spin-echo experiment with four transients for each value of the delay. This sequence comprises a $(\pi/2)_x$ pulse, a delay, a $(\pi)_x$ pulse applied at the same rotor orientation ($\pm 0.5^\circ$) as the $(\pi/2)_x$ pulse, and a further delay before

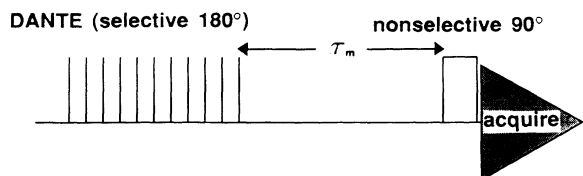


FIG. 2. SPARTAN pulse sequence for measuring spectral spin diffusion (see text).

acquisition. Synchronization was necessary to ensure that the second pulse comes at the maximum of a rotational echo.¹⁸ The value of T_2 was obtained by fitting the peak heights to an exponential using Varian VNMR 2.2 software.

^{19}F MAS-NMR spectral spin diffusion was measured by selective inversion of a specific resonance and its associated sidebands, followed by a cross-relaxation delay, and then a nonselective $\pi/2$ pulse to monitor the longitudinal magnetization (Fig. 2). Selective inversion of the center band and sidebands was achieved by a DANTE pulse train²⁷ that consisted of fifteen 12° ($1.6\text{-}\mu\text{s}$) pulses applied once a rotor period at identical rotor orientations (to within $\pm 0.5^\circ$). These pulse lengths (and the corresponding power levels) were chosen to give an optimal excitation profile for the peaks in the spectra. The nonselective $\pi/2$ observation pulse was $12\ \mu\text{s}$, and its phase was alternated to cancel out the effects of DANTE pulse trains that did not fully invert the magnetization of a specific resonance.²⁸ The cross-relaxation mixing period was varied from 1 ms to 12 s, with eight transients collected for each mixing time.

Deconvolution of overlapping ^{19}F MAS-NMR peaks was performed using the standard deconvolution tools in VNMR 2.2, the software package on the Varian VXR-400 spectrometer. This program operates by fitting the spectrum to a set of user-selected Lorentzian peaks by optimizing the linewidths, chemical shifts, and peak intensities.

III. RESULTS

A. ^{31}P MAS-NMR

The ^{31}P MAS-NMR spectrum of fluorapatite is shown in Fig. 3(a). It contains a peak at the isotropic chemical shift of 2.8 ppm with a half-height linewidth (HHLW) of 0.4 ppm and small sidebands arising from a small chemical-shift anisotropy.¹¹ The spectrum of fluorapatite containing 2.1 wt % antimony is shown in Fig. 3(b). There are no additional peaks observed in the spectrum of antimony-doped fluorapatite with enough intensity to be attributable to the presence of antimony (i.e., if each antimony ion perturbed five phosphorus atoms, e.g., by occupying a calcium site, the corresponding perturbed ^{31}P peak would have 15.1% of the total spectral intensity). The small peaks shown in the expansion of Fig. 2(b) at approximately -9 ppm can be attributed to a very minor pyrophosphate-impurity phase. The ^{31}P MAS-NMR spectrum of antimony phosphate (SbPO_4) is shown in Fig. 3(c). A rather broad peak ($\Delta\nu_{1/2}=4.0$ ppm) with an isotropic chemical shift of -18.3 ppm and weak sidebands is seen.

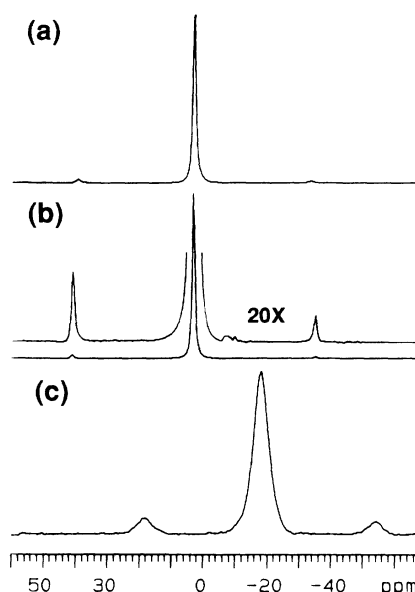


FIG. 3. ^{31}P MAS-NMR spectra with $\nu_r=6.15\pm 0.1$ kHz: (a) pure fluorapatite; (b) fluorapatite containing 2.1 wt % antimony(III) dopant, 20 \times vertical expansion above; and (c) SbPO_4 .

To test the effect of substituting different group-II metal ions in the Ca sites, ^{31}P MAS-NMR spectra of $\text{Sr}_{1.03}\text{Ca}_{8.97}\text{F}_2(\text{PO}_4)_6$, $\text{Sr}_5\text{F}(\text{PO}_4)_3$, and $\text{Ba}_5\text{F}(\text{PO}_4)_3$ were obtained. The spectrum of $\text{Sr}_{1.03}\text{Ca}_{8.97}\text{F}_2(\text{PO}_4)_6$ contains a peak with an isotropic chemical shift of 3.3 ppm, with an upfield shoulder at 2.4 ppm. The spectrum of $\text{Sr}_5\text{F}(\text{PO}_4)_3$ contains a peak with an isotropic chemical shift of 3.3 ppm. The spectrum of $\text{Ba}_5\text{F}(\text{PO}_4)_3$ contains a major peak at 1.4 ppm and two weaker peaks, the first at 2.3 ppm with $\frac{1}{12}$ the intensity of the main and the second (a weak shoulder) at 0.5 ppm, both presumably arising from impurities.

B. ^{19}F MAS-NMR

The ^{19}F MAS-NMR spectrum of fluorapatite is shown in Fig. 4(a). The isotropic chemical shift is 64.2 ppm, and the $\Delta\nu_{1/2}$ is 0.5 ppm. The sidebands of fluorapatite in the ^{19}F MAS-NMR spectrum arise principally from the axially symmetric chemical-shift tensor [the anisotropy has been reported as 84 and 85 ppm (Refs. 29 and 30)], although the ^{19}F - ^{19}F dipolar couplings³¹ and to a lesser extent ^{19}F - ^{31}P dipolar couplings also contribute. The ^{19}F MAS-NMR spectrum of fluorapatite with 2.1 wt % antimony is shown in Fig. 4(b). This spectrum contains an intense resonance at 64.2 ppm and its associated sidebands, similar to those of fluorapatite, as well as three new peaks at 73.1, 68.6, and 65.6 ppm. The 65.6-ppm peak is a shoulder of the main peak at 64.2 ppm, but is resolved by difference spectroscopy, as discussed below. Since peaks at (or near) 68.6 and 65.6 ppm are observed in the spectra of *all* of the samples containing antimony, we will refer to them throughout this paper as peaks *A* and *B*, respectively. The large main peak at (or near) 64.0

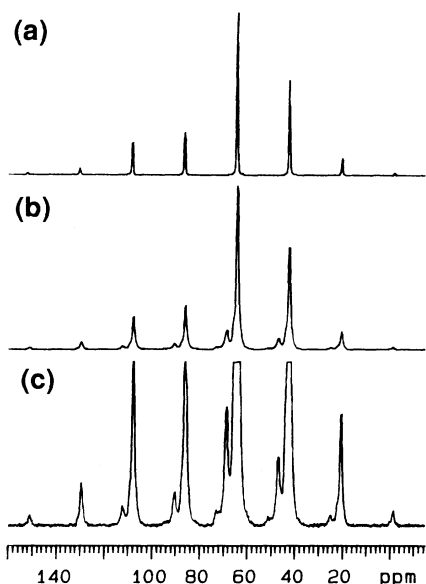


FIG. 4. ^{19}F MAS-NMR spectra with $\nu_r = 8.25 \pm 0.1$ kHz: (a) fluorapatite, (b) fluorapatite containing 2.1 wt % antimony(III), and (c) vertical expansion of spectrum in (b).

ppm will be referred to as peak *C*. Because of its overlap with peak *C*, the chemical shift of peak *B* is less accurately determined than those of peaks *A* and *C*. The weak, broad peak at 73.1 ppm is present only in the ^{19}F MAS-NMR spectra of the samples containing 1.3, 1.7, and 2.1 wt % antimony. All of the spectra of fluorapatite containing antimony have a very small upfield shoulder on peak *C*. Deconvolution indicates that the intensity of this shoulder is less than $\frac{1}{100}$ the intensity of peaks *A* and *B*, implying that this peak does not arise from the same source as *A* and *B*. Since the shoulder is so weak, we will not discuss it further. The chemical shifts, linewidths, and intensities (as a percentage of the total intensity) obtained from deconvolution of the peaks in each of the ^{19}F MAS-NMR spectra as well as the spin-lattice relaxation times (T_1) are given in Table I.

It has been demonstrated³² that random molecular (or atomic motions) can interfere with coherent NMR-line-narrowing techniques such as MAS, resulting in broadening of lines if the MAS rotor period is comparable to the

molecular-correlation time. In order to demonstrate that random atomic motion is not broadening any of the peaks in the ^{19}F MAS-NMR spectrum to the point where they are undetectable, the spectrum of fluorapatite containing 1.7 wt % antimony was obtained at 223 K. Since there is no difference between the spectrum obtained at 223 K and the one obtained at 295 K, random atomic motions do not appear to be interfering with the MAS process and producing broadened peaks.

In order to obtain more accurate chemical-shift, linewidth, and intensity measurements of the shoulder corresponding to peak *B* in the spectra of doped fluorapatite, difference spectroscopy was used for all samples. Figure 5 is a ^{19}F MAS-NMR difference spectrum obtained from the spectrum of fluorapatite containing 2.1 wt % antimony and the spectrum of pure fluorapatite. Because the chemical shift of peak *C* in the doped sample is 0.2 ppm upfield of the chemical shift of fluorapatite, the difference spectrum was obtained by varying the frequency offset, linewidth (exponential apodization), and intensity (scaling factor) of the pure fluorapatite spectrum to provide the best null of the center band of peak *C*. The amount of applied line broadening (apodization) required to make the linewidth of the center band in the fluorapatite spectrum equal to the linewidth of peak *C* in each spectrum of fluorapatite containing antimony increased monotonically with the amount of antimony incorporated into the lattice. This suggests that the presence of antimony in the lattice slightly perturbs the apatitic fluoride ions which give rise to peak *C*, resulting in a symmetrical line broadening (the specific surface areas of the 0.0- and 2.1-wt % Sb samples are similar, arguing against crystal-size effects being responsible). The additional line broadening applied to the fluorapatite spectrum to achieve nulling of peak *C* in the difference spectrum does not result in a significant reduction of the intensity of peak *B* in the difference spectrum since the applied broadening is small (between 0.1 and 0.8 ppm) compared to the chemical-shift difference between peaks *B* and *C* (1.6 ppm). The difference spectrum clearly shows distinct peaks for *A* and *B*. The ratio of the intensity of peak *A* to peak *B*, determined by integration, equals 2:1 to within 16% uncertainty for all samples (except the 0.18-wt % sample). The deviation of this ratio from 2:1 becomes less with increased dopant levels, presumably

TABLE I. ^{19}F MAS-NMR data for antimony(III)-doped fluorapatite samples.

wt % antimony (III)	Peak at ~73 ppm		Peak <i>A</i> (chemical shift, HHLW, area) ^a	Peak <i>B</i> (chemical shift, HHLW area) ^a	Peak <i>C</i> (chemical shift, HHLW, area) ^a
	T_1 peak <i>A</i> (s)	T_1 peak <i>C</i> (s)			
0					64.2, 188, (100)
0.18	278±53	228±12		68.8, 180, 1.1	64.2, 155, 98.7
0.8	132±11	123±4		68.2, 361, 6.6	63.6, 254, 91.4
1.3	378±10	369±8	72.6, 416, 0.5	68.2, 467, 8.8	63.5, 341, 86.3
1.7	193±7	175±8	72.6, 2285, 4.7	68.2, 380, 7.6	63.6, 282, 83.5
2.1	222±12	183±13	73.1, 1092, 3.2	68.6, 633, 13.6	64.0, 387, 73.1
3.0	247±33	218±13		68.8, 329, 5.0	64.2, 248, 94.2

^appm (with respect to hexafluorobenzene); Hz; percentage of total.

^bBecause of the weakness of this peak, the HHLW was set to this value to obtain a reasonable fit.

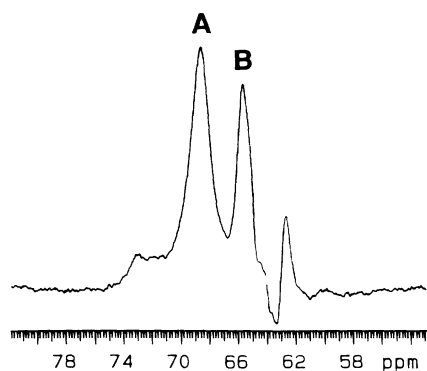


FIG. 5. ^{19}F MAS-NMR difference spectrum of fluorapatite containing 2.1 wt % antimony(III) and undoped fluorapatite (see text).

because the correspondingly greater intensity of peaks *A* and *B* results in less uncertainty in their integrated areas.

The relative intensities of the sidebands of peak *C* in the ^{19}F MAS-NMR spectra of the samples of fluorapatite containing antimony are similar to those in the spectrum of fluorapatite, but the intensity of the third left sideband of peak *C* (in the sample containing 2.1 wt % antimony) is only 70% of that of the corresponding sideband in pure fluorapatite.

The vertically expanded center-band regions of the ^{19}F MAS-NMR spectra of each of the antimony-doped fluorapatite samples as well as that of the undoped sam-

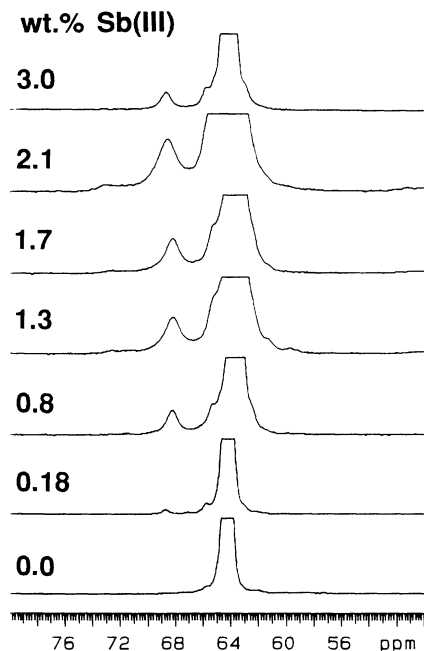


FIG. 6. ^{19}F MAS-NMR spectra (center-band region only) of antimony(III)-doped fluorapatite samples, $\nu_r = 8.25 \pm 0.1$ kHz, weight percent of antimony as indicated. The height of the main apatite peak (off scale) is equal for all spectra.

ple are shown in Fig. 6. The heights (off scale) of peak *C* for each of these spectra were set equal. The intensity of the peaks *A* and *B* associated with the presence of antimony in the sample do not monotonically increase with the weight percent of *total* antimony, since not all of the antimony is present in the site responsible for these peaks (see below).

The T_1 values for peak *C* given in Table I are the average of the (nearly identical) T_1 values for the center band and the first right and first left sideband. The T_1 values for peak *A* are simply the T_1 values of the center band. The T_1 values of peak *B* for the various samples are not reported, since this peak severely overlaps peak *C*. Furthermore, the T_1 values of the 73.1-ppm peak are not reported since the intensity of this peak is too small. Nevertheless, the T_1 values of peak *B* and the 73.1-ppm peak are very close to that of peak *C* in a given sample, since their intensities follow the intensity of the main peak *C* for various delay times in the inversion-recovery experiments. The spin-lattice relaxation times of peaks *A*, *B*, *C*, and the peak at 73.1 ppm are nearly equal to within experimental error for each sample; however, they vary irregularly from 129 to 378 s, with no perceptible relationship to the antimony content.

The measured ^{19}F MAS-NMR transverse relaxation times (T_2) of peak *C* in the samples containing 2.1 and 1.7 wt % Sb are 32 and 40 ms, respectively. These T_2 values would contribute 10 Hz (0.027 ppm) to the linewidth of peak *C* for the sample containing 2.1 wt % antimony and 8 Hz (0.021 ppm) for the sample containing 1.7 wt % antimony. The external magnetic field was shimmed by minimizing the proton linewidth of water in a spinning MAS rotor, yielding an estimated contribution to the half-height linewidth from field inhomogeneity of about 20 Hz (0.053 ppm). The observed half-height linewidths of the samples are considerably greater than the sum of the homogeneous broadening and the contribution from field inhomogeneity (~ 0.1 ppm); they vary from 0.5 to 1.0 ppm (Table I). These half-height linewidths are significantly less than those previously reported for fluorapatite,^{12,33} possibly because the fluorapatite in the earlier study was synthesized by an aqueous precipitation method.

Figure 7 shows the ^{19}F MAS-NMR spectra of fluorapatite containing 1.7 wt % antimony obtained using the SPARTAN pulse sequence. The frequency selectivity of the DANTE train was adjusted so that peak *A* would be inverted and the other peaks would remain unperturbed. The negative longitudinal magnetization of the inverted peak *A* comes to quasiequilibrium with the relatively large bath of positive magnetization in the main apatite peak *C* in approximately 12 s (a time much less than the measured spin-lattice relaxation time of 193 s). While the height of the main peak decreases noticeably, the height of peak *B* remains constant. The total integral of the center-band region containing peaks *A*, *B*, and *C* should remain constant if spin diffusion is the only process affecting peaks *A*, *B*, and *C*. Measurements of the integral of this region show a 1.5% increase from short to long mixing times, which is the amount expected from spin-lattice relaxation. To obtain the spin-diffusion time

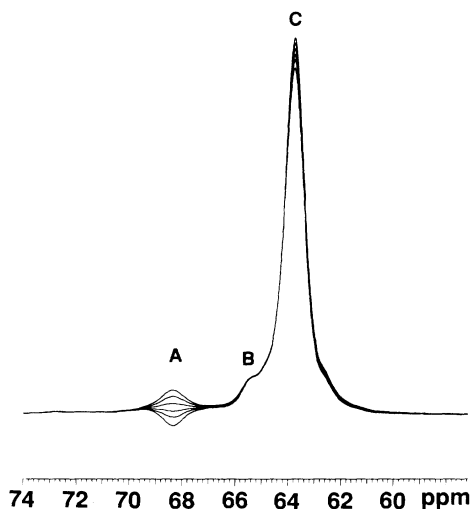


FIG. 7. ^{19}F MAS-NMR spectra (center-band region only) obtained using the SPARTAN pulse sequence (Fig. 2 and text) of fluorapatite containing 1.7 wt % antimony(III). Spectra for cross-relaxation mixing periods of 0.1, 0.5, 1, 2, 4, and 12 s are superimposed. Peak *A* (at 68.6 ppm) is inverted at short mixing periods, and peak *C* (at 64.0 ppm) steadily decreases in intensity for longer mixing periods.

constant from the spectra in Fig. 7, we have adapted the analysis in Ref. 34 for the present experiment. Although the data could be treated by simply fitting the magnetizations of peaks *A* and *C* to simple exponential curves, this method provides a concise way of incorporating both data sets into one plot. The spin-diffusion time constant is obtained by plotting $\ln[(rf+f)/r]$ vs τ_m (mixing time). The f in this relationship is given by the equation

$$f = \frac{M_A(\tau_m = \infty) - M_A(\tau_m = 0)}{M_A(\tau_m = \infty)}, \quad (1)$$

where $M_A(\tau_m = \infty)$ and $M_A(\tau_m = 0)$ are the intensities of peak *A* obtained from an exponential fit. In this relationship r is given by the equation

$$r = \frac{M_A(\tau_m)}{M_C(\tau_m) - M_C(\tau_m = \infty)}, \quad (2)$$

where $M_A(\tau_m)$ is the integrated intensity of peak *A*, $M_C(\tau_m)$ is the integrated intensity of peak *C*, and $M_C(\tau_m = \infty)$ is the intensity of peak *C* at infinite mixing time obtained from an exponential fit. Contributions to $M_C(\tau_m)$ and $M_A(\tau_m)$ from the much slower longitudinal relaxation process can be safely neglected. The plot, shown in Fig. 8, should be linear for a process governed by a single spin-diffusion rate, with the slope of the line equal to the reciprocal of the spin-diffusion time constant, $1/\tau_{\text{SD}}$. The slopes of the plots were determined by fitting the data to a line, weighting points inversely proportional to their variances squared. The values of τ_{SD} for the data sets shown in Fig. 8 are 0.68 ± 0.04 s for $\nu_r = 5.09$ kHz, 1.79 ± 0.11 s for $\nu_r = 6.98$ kHz, and 2.22 ± 0.10 s for $\nu_r = 9.23$ kHz. The error values given are one standard deviation of τ_{SD} as determined by weighted regression.

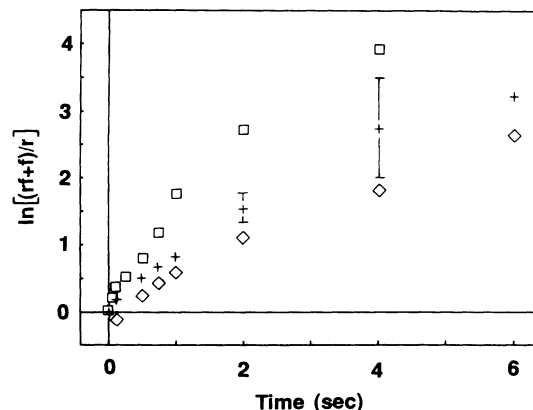


FIG. 8. Measurement of spin-diffusion rates between peaks *A* and *C* in the ^{19}F MAS-NMR spectra of fluorapatite containing 1.7 wt % antimony at three different spinning speeds using the SPARTAN pulse sequence: $\ln[(rf+f)/r]$ vs τ_m (see text). $\nu_r = 9.23$ kHz (\diamond), 6.98 kHz (+), and 5.09 kHz (\square). Representative error bars are included on two of the data points.

To show convincingly that there is no spin diffusion between peaks *A* and *B*, the SPARTAN pulse sequence was also used on the fluorapatite sample containing 0.8 wt % antimony, since peak *B* was most well resolved for this sample. As with the 1.7-wt % sample, the height of the main peak *C* decreases noticeably as peak *A* becomes positive and peak *B* remains constant within experimental error. The spin-diffusion time constant for this sample was 1.95 ± 0.31 s for $\nu_r = 9.26$ kHz.

To test the effect of temperature on the spin-diffusion rate, the SPARTAN experiment was performed on the sample containing 1.7 wt % antimony at a temperature of 223 K and a $\nu_r = 8.10$ kHz. The measured rate of spin diffusion between peaks *A* and *C* at the lower temperature was essentially unchanged ($\tau_{\text{SD}} = 1.89 \pm 0.12$ s).

Attempts to monitor spin diffusion by inverting peak *B* and observing cross-relaxation to the other peaks were unsuccessful since no combination of pulse lengths or power levels was found that could selectively invert peak *B* without significantly exciting peak *C*.

IV. DISCUSSION

The discussion portion of this paper is divided into three sections. The first section discusses the basic principles of spectral spin diffusion and shows how the experimental results involving spin diffusion enable one to assign the ^{19}F MAS-NMR peaks to specific antimony-perturbed fluoride ions in the apatite lattice. The second section first demonstrates that potential effects upon the MAS-NMR spectra arising from the presence of quadrupolar antimony nuclei do not appear, as a result of rapid relaxation of the quadrupolar nuclei. It then discusses the quantitative aspects of the ^{19}F MAS-NMR spectra and the agreement between the NMR and ir results regarding the amount of antimony actually incorporated into the apatite lattice. In the third and final section, the phosphate site is shown to be the only location for antimony in the fluorapatite lattice that is consistent with

all of the experimental MAS-NMR results. Molecular modeling of the apatite lattice leads to a plausible assignment of the ^{19}F MAS-NMR spectra.

A. Spin diffusion

Spin diffusion is a term used to describe the transfer of longitudinal (z) magnetization within a homonuclear spin system between different regions of sample via the dipole-dipole coupling of nuclear spins.^{35,36} The process is often assumed to exhibit general Fickian-diffusion behavior, although we need make no such assumptions here, especially since our system is basically one dimensional. Spin diffusion allows paramagnetic centers or mobile domains to act as relaxation sinks for spins throughout the sample and can manifest itself as a nonexponential spin-lattice relaxation process.^{35,36} Spectral spin diffusion refers to the situation where the spins have different resonance frequencies³⁷ and is usually observed in single crystals or under MAS conditions. The transfer of polarization is accomplished by the simultaneous exchange of Zeeman magnetization between two adjacent spins, a process usually referred to as a spin "flip-flop." One manifestation of spectral spin diffusion is an equalization of the longitudinal relaxation times of spectrally resolved spins.³⁸ In a limited number of cases, spectral spin diffusion in solids has been observed directly by selectively inverting the magnetization of one peak and monitoring cross-relaxation to other peaks.^{24,25,28,39-41}

Spectral spin diffusion can occur provided interspin flip-flops conserve the total Zeeman energy. Sources of energy that can balance any mismatch in the Zeeman energies include large extraneous dipolar-spin reservoirs, such as abundant protons,^{24,28,40-43} external radio-frequency fields,⁴⁴ and coupling between the spin system and rotation of the sample.^{28,38,42,45,46} None of the spectra reported here were obtained under such conditions.

Kubo and McDowell²⁸ have pointed out that scalar coupling can facilitate spin diffusion under MAS conditions. Through-space scalar couplings between ^{19}F nuclei have been reported to be as large as 217 Hz.^{47,48} Since the intensity of peak *A* in the Hahn spin-echo experiments was observed to decay monotonically with a time constant (T_2) of 34 ms, any scalar coupling to a neighboring C fluorine nucleus must be less than approximately 15 Hz. Since the magnitude of the scalar coupling (< 15 Hz) is substantially less than the dipolar coupling (see below), spin diffusion must proceed predominantly through the dipolar interaction.

It is conceivable that atomic motions with spectral density at the frequency difference between peaks *A* and *C* could provide energy to compensate for the Zeeman mismatch between these peaks and thus facilitate spin diffusion. The fact that the spin-diffusion rate is essentially unchanged at lower temperatures indicates that, if such a mechanism is responsible for the observed spin diffusion, the motion must have an activation barrier less than kT .

Kubo and McDowell²⁸ have pointed out that only if two identical chemical shielding tensors of neighboring spins have the same orientation will there generally be efficient spin diffusion. This situation certainly applies to

the unperturbed fluorine nuclei in the fluorapatite lattice, whose axially symmetric shift tensors have their principal axes along the c axis of the crystal. However, spin diffusion in MAS-NMR spectra can occur, albeit less efficiently, even if the chemical shielding tensors have a different orientation or are unequal. For spin diffusion to occur under such conditions, without other sources to provide for Zeeman mismatch, level crossing must take place.²⁸ A similar enhancement of spin diffusion by level crossing during sample rotation for quadrupolar powder patterns of deuterium nuclei has been reported by Eckman.⁴⁹ Since the frequency of each of the resonances varies during the rotor cycle,^{50,51} level crossing can occur when the two frequencies coincide.

The effects of spectral spin diffusion provide information as to whether peaks *A*, *B*, and the peak at 73.1 ppm in the ^{19}F MAS-NMR spectra of antimony-containing fluorapatite arise from fluorine atoms in the apatite lattice or in secondary, nonapatitic phases. Since the ^{19}F T_1 values vary greatly (and irregularly) among the antimony-containing fluorapatite samples (130–380 s), the primary source of longitudinal relaxation is probably paramagnetic impurities introduced during synthesis and not intrinsic lattice motions. When paramagnetic species are present, the magnetization recovery is expected to be,³⁵ and has been observed to be, nonexponential. However, the T_1 values reported in Table I were obtained by fitting the relaxation data to a single exponential, which appeared to provide a good fit (no significant breaks in the logarithmic plot of the relaxation data were observable).

The fact that the T_1 values of peaks *A*, *B*, *C*, and the 73.1-ppm peak are nearly identical within experimental error suggests that the spins corresponding to these peaks are in spin-diffusion contact with each other over the long-time scale of T_1 (but see below). This implies that the corresponding spins are in the same crystallites and not in different (secondary) phases. The rate of spin diffusion depends upon, among other factors, the square of the dipolar-coupling constant between pairs of spins.³⁶ Fluorapatite contains parallel linear chains of fluoride ions with intrachain fluorine atoms 344 pm apart and with an interchain closest fluorine-fluorine distance of 937 pm. The corresponding calculated maximum homonuclear dipolar couplings (internuclear vector parallel to the magnetic field) are 5234 and 262 Hz, respectively. The largest fluorine-phosphorus dipolar coupling is ca. 2200 Hz, and the largest phosphorus-phosphorus dipolar coupling is ca. 640 Hz. The spin diffusion that we observe in the present system is for a spinning speed (up to 9.23 kHz) significantly exceeding the largest dipolar coupling in the spin system. Spin diffusion has been reported to be quenched by MAS spinning speeds that exceed the dipolar couplings,⁴² but the quantitative degree of reduction in rate or quenching in this case has apparently not been studied experimentally.

Spectral spin diffusion among peaks in the ^{19}F MAS-NMR spectrum is most likely made possible by an instantaneous match of the frequencies of the spins of two peaks due to differences in the chemical shielding tensors of the spins (see above). The isotropic chemical shifts of

peaks *A* and *C* differ by 4.6 ppm, which is only a small fraction of the total chemical-shift anisotropy of 84 or 85 ppm.^{29,30} Thus it is plausible that the frequencies could match during the rotor cycle. Although it was not possible to accurately determine the components of the chemical shielding tensors of peaks *A*, *B*, and *C*, the slight differences in sideband intensities of peaks *A* and *C* suggest a difference in the chemical-shift anisotropy of each peak.⁵² The increase in the spin-diffusion rates between peaks *A* and *C* at lower spinning speeds is expected since the zero-quantum linewidth would be greater at lower spinning speeds,²⁸ thus increasing the time during which the zero-quantum linewidths of peaks *A* and *C* overlap during a given rotor period.

The spectral spin-diffusion results obtained using the SPARTAN sequence allow assignments of peaks *A*, *B*, and *C*. Figure 9 shows a geometrical arrangement of the fluorine nuclei of peaks *A* and *B* in the fluorapatite lattice that explains both the observed spin diffusion between peaks *A* and *C* and the considerably reduced spin diffusion between peaks *A* and *B*. The model also takes into account the 2:1 intensity ratio of peaks *A* and *B* discussed in Sec. IV B. In this arrangement the fluorine nuclei of peaks *A* and *C* are neighboring, with no intervening peak *B* nuclei, thus permitting facile spin diffusion. Since peaks *A* and *B* arise from fluorine nuclei in different chains, direct spin diffusion between these peaks would be negligible; instead, spin diffusion would proceed indirectly and more slowly through the nuclei of peak *C*. We should note that a model in which the two fluorine nuclei of peak *A* are on *different* chains would also be consistent with the spin-diffusion results; however, structurally this model is less plausible (see Sec. IV C 1).

B. Quantitative aspects of ^{19}F MAS-NMR results and extent of antimony incorporation

In order to obtain quantitative information about the amount of antimony in the fluorapatite lattice through its effect on the ^{19}F MAS-NMR spectrum, it is important to consider the effect that the quadrupolar antimony nucleus could have on the spectrum of the spin- $\frac{1}{2}$ fluorine nucleus. Antimony has two quadrupolar isotopes: ^{121}Sb

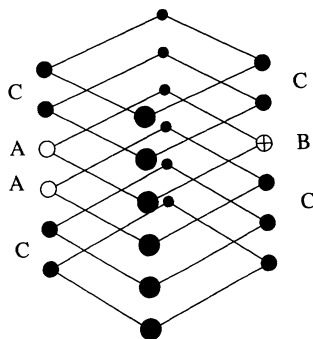


FIG. 9. Schematic diagram as in Fig. 1, showing the arrangements of fluoride ions giving rise to peaks *A* and *B* in the ^{19}F MAS-NMR spectra. The antimony atom (not shown) is between the fluoride ions labeled *A* and *B* (see also Fig. 12).

with $I = \frac{5}{2}$ and a natural abundance of 57.25% and ^{123}Sb with $I = \frac{7}{2}$ and a natural abundance of 42.75%. Effects of half-integral quadrupolar nuclei on the spectrum of a spin- $\frac{1}{2}$ nucleus under MAS conditions have been observed experimentally and calculated theoretically.^{53–55} Generally, magic-angle sample spinning fails to eliminate the effect of dipolar coupling on the spectrum of a spin- $\frac{1}{2}$ nucleus dipolar coupled to a quadrupolar nucleus, because the axis of quantization of the quadrupolar spin is not parallel to H_0 . The MAS-NMR spectrum of a spin- $\frac{1}{2}$ nucleus dipolar coupled to a quadrupolar nucleus is usually a complicated powder pattern with singularities, whose total breadth is roughly on the order of the dipolar coupling between the spin- $\frac{1}{2}$ and quadrupolar nuclei. The details of the pattern are governed by the sign and magnitude of the nuclear quadrupole-coupling constant, the nuclear spin, and the angles between the principal axes of the dipole and quadrupolar interaction tensors.⁵³ The nuclear quadrupole-coupling constant of the ^{121}Sb nucleus in fluorapatite has been measured to be approximately 700 MHz.⁵

For antimony nuclei in any of the proposed substitution sites, significant dipolar couplings to both fluorine and phosphorus nuclei would be expected to produce observable quadrupolar effects in the ^{19}F and ^{31}P MAS-NMR spectra. The calculated dipolar couplings between an ^{121}Sb (^{123}Sb) antimony nucleus occupying the Ca(2), Ca(1), or phosphate site and the nearest fluorine nucleus in the fluorapatite lattice are 2.45 kHz (1.33 kHz), 161 Hz (87 Hz), and 630 Hz (340 Hz), respectively. If antimony nuclei were producing quadrupolar effects upon the ^{19}F MAS-NMR spectra, peaks *A* and *B* would be much broader than peak *C*; however, only peak *A* is slightly broader, and we ascribe this to the presence of two slightly different isotropic chemical shifts (see Sec. IV C 3). Furthermore, if peak *A* or *B* were influenced by dipolar coupling to antimony, they would not be simple Lorentzian peaks, but rather complicated powder patterns.⁵³ The peak at 73.1 ppm and peaks *A* and *B* in the ^{19}F MAS-NMR spectra of antimony-doped fluorapatite are not part of such a powder pattern, because the intensity of the 73.1-ppm peak varies independently of the intensity of peaks *A* and *B* for the various samples.

Paralleling the ^{19}F MAS-NMR results, the ^{31}P MAS-NMR spectra of antimony-doped fluorapatite samples fail to exhibit any quadrupolar effects. The peak at the isotropic chemical shift of fluorapatite is not broadened at the base; nor is its half-height linewidth significantly greater than that of undoped fluorapatite. The most probable explanation for the lack of an effect by the quadrupolar antimony nuclei on the ^{19}F and ^{31}P MAS-NMR spectra is “self-decoupling” due to rapid spin-lattice relaxation ($T_1 \approx 1 \times 10^{-4}$ s) of the antimony nuclei.⁵³

In the ^{31}P MAS-NMR spectrum of SbPO_4 , the isotropic peak has a $\Delta\nu_{1/2}$ of 4 ppm, about 10 times greater than that of fluorapatite. The increased linewidth in this case may arise from the above quadrupolar effect upon the phosphorus nuclei dipolar coupled to antimony nuclei; presumably, in this case, the antimony spin-lattice relaxation time is insufficiently short for complete “self-

decoupling" to occur.

Having demonstrated the absence of quadrupolar effects upon the MAS-NMR spectra of antimony-doped fluorapatite, we will now discuss the relative intensity of the ^{19}F MAS-NMR peaks in relation to the amount of antimony present. Figure 10 is a plot, from the deconvolution data given in Table I, of the intensity of peak *A* in the ^{19}F MAS-NMR spectra versus the total weight percent of antimony of the samples. The lack of a meaningful correlation indicates that some antimony must go into a secondary phase or a site in the fluorapatite lattice other than the one giving rise to peak *A*. In the samples containing 1.3, 1.7, and 2.1 wt % antimony, the antimony not associated with peak *A* is most likely in a site in the fluorapatite lattice that gives rise to the peak at 73.1 ppm, as will be discussed in Sec. IV C 3. Since the ^{19}F and ^{31}P MAS-NMR spectra of the sample containing 3.0 wt % antimony do not contain peaks with enough intensity to account for the antimony that is not associated with peak *A*, the "missing" antimony must be in a phase that does not contain fluorine or phosphorus. X-ray powder-diffraction data (of the identical 3.0-wt % antimony sample used in this study) suggest that this phase is calcium meta-antimonate.

The solid line in Fig. 10 is the theoretical relationship expected if two fluorine nuclei are affected by each antimony atom in the lattice and all of the antimony is incorporated into the lattice. Since two of the samples (0.18 and 0.8 wt %) have peak-*A* intensities on or near this line, there are most likely *two A* fluorine atoms affected per incorporated antimony atom. It is unlikely that peak *A* arises from three or more fluorine atoms per incorporated antimony atom for several reasons. The amount of incorporated antimony as determined by ir (see next paragraph) for numerous samples containing less than 0.8 wt % antimony is proportional to the total antimony content,⁵⁶ suggesting that all of the antimony

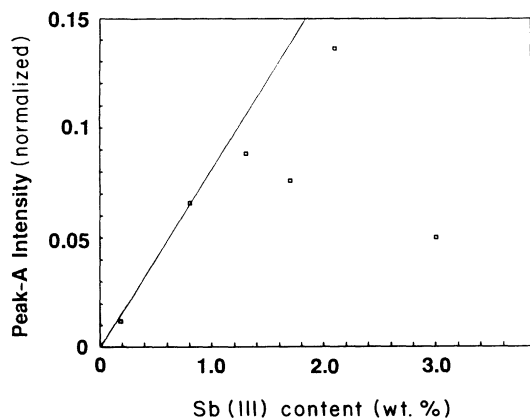


FIG. 10. Plot of the ^{19}F MAS-NMR intensity of peak *A* obtained from deconvolution (see Table I) expressed as the fraction of the total intensity vs the weight percent of antimony(III). Data were obtained from spectra in Fig. 6. Solid line is theoretical plot, with two assumptions: that peak *A* arises from two fluorine atoms per antimony atom and that all of the antimony is incorporated into the apatite lattice.

present at these relatively low concentrations is incorporated into the apatite lattice. Furthermore, [fluorine *A*]/[Sb] molar ratios greater than 2:1 are difficult to reconcile with any of the models of antimony substitution discussed in Sec. IV C. Since the ratio of the area of peak *A* to peak *B* is 2:1 from the difference-spectroscopy results, we can conclude that peak *B* arises from *one* fluorine nucleus perturbed by each antimony atom in the lattice.

The fluorescence of antimony-doped fluorapatite has been shown to be directly proportional to a specific peak in the ir spectrum at 686 cm^{-1} .⁸ The intensity of this ir band can therefore be used to determine the mole fraction of (fluorescence-active) antimony in the lattice of a given sample, using the 0.8-wt % sample as a calibration standard (assuming that all antimony in this sample is incorporated into the lattice, as the above paragraph indicates). Figure 11 is a plot from the deconvolution data given in Table I of the intensity of peak *A* in the ^{19}F MAS-NMR spectra versus the mole fraction of antimony in the lattice as determined by ir. The mole fraction antimony is calculated using the defect formula $\chi_{\text{Sb}} = [\text{mol Sb}]/[\text{mol Ca}_5\text{F}(\text{PO}_4)_{3-x}(\text{SbO}_3)_x]$. The linearity of this plot not only confirms that peak *A* arises from antimony incorporated into the apatite lattice, but more importantly demonstrates that this peak is related to the specific antimony site responsible for fluorescence. The slope of the plot in Fig. 11 is 1.97 ± 0.18 , or approximately 2, indicating that there are two fluorine nuclei affected by each antimony atom in the lattice.

C. Antimony-substitution sites

In order to make specific assignments of peaks *A* and *B* in the ^{19}F MAS-NMR spectra of antimony-doped fluorapatite, we must consider which of the possible antimony-substitution sites can account for all of the experimental results. The antimony-substitution site must be close enough to two apatitic fluorine nuclei to significantly perturb their ^{19}F chemical shifts and must produce an equal or nearly equal perturbation (since peak

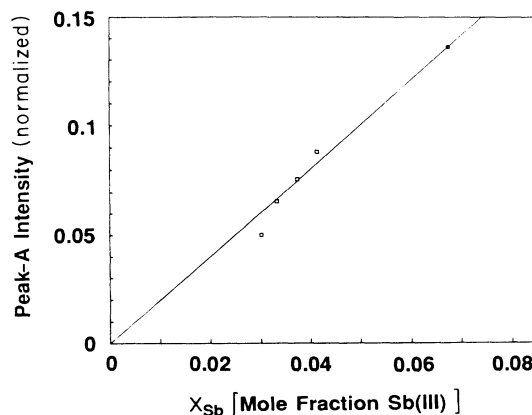


FIG. 11. Plot of ^{19}F MAS-NMR intensity of peak *A* as in Fig. 10 vs the mole fraction of antimony incorporated into the apatite lattice as determined by ir (see text).

A is a single peak 4.6 ppm from the main apatite peak). It must also be close enough to a single fluorine nucleus to slightly perturb its ^{19}F chemical shift (since peak *B* is 1.6 ppm from the main apatite peak). As discussed in Sec. IV A the fluorine nuclei giving rise to peaks *A* and *B* must be in different fluorapatite chains. Finally, the substitution site of antimony must produce a negligible perturbation of the ^{31}P chemical shift.

Simulations of ^{31}P MAS-NMR spectra of the 2.1-wt % sample show that, if each antimony atom were to perturb three phosphorus nuclei (the smallest number of neighboring phosphorus atoms an antimony atom would have in any substitution site), a chemical-shift perturbation of 0.4 ppm would be easily detectable as a shoulder on the main apatite peak. Although the effects upon the ^{31}P chemical shift of replacing calcium in the fluorapatite lattice by strontium or barium are rather small (< 2 ppm), unlike antimony, these ions have the same charge as calcium. Turner *et al.*⁵⁷ have shown an approximate empirical correlation of the ^{31}P chemical shift in metal phosphates with the quantity $Zr^{-1/2}$, where *Z* is the formal cation charge and *r* its ionic radius. Neglecting the structural differences between compounds, this correlation rationalizes the much larger effect upon the ^{31}P chemical shift of replacing Ca^{2+} ($Z=2$, $r=99$ pm) by Sb^{3+} ($Z=3$, $r=76$ pm) rather than Sr^{2+} ($Z=2$, $r=112$ pm) or Ba^{2+} ($Z=2$, $r=134$ pm).⁵⁸

The ^{31}P chemical shift of antimony phosphate, which has four antimony(III) atoms bonded to each phosphate tetrahedron,⁵⁹ is -18.3 ppm. If an antimony atom occupies a calcium site in the apatite lattice, it would be adjacent to a phosphate tetrahedron. The Sb-O-P linkage would then be expected to produce a detectable difference in the ^{31}P MAS-NMR spectrum, on the order of 5 ppm ($\frac{1}{4}$ of the difference between the ^{31}P chemical shift of FAP and that of SbPO_4).

In the following three sections, we will discuss the three proposed sites for antimony substitution in light of the combined ^{19}F and ^{31}P MAS-NMR results.

1. Ca(1) site

Previous studies have provided evidence against the Ca(1) site as the antimony-substitution site.^{5,9} The lack of axial symmetry for the antimony nuclear quadrupole-coupling constant obtained from Mössbauer spectroscopy has been used to argue against the Ca(1) site, which has threefold symmetry in the apatite lattice. However, although not explicitly discussed, the mechanism of charge compensation must be considered. If antimony occupied the Ca(1) site, charge balance would most likely be accomplished either by removing two Ca(1) ions [or alternatively one Ca(1) ion and one Ca(2) ion] and one fluoride ion or by removing one Ca(1) ion and replacing a fluoride ion with an O^{2-} ion. In both cases the antimony atom would reside in the center of a triangular prism formed from three columns of fluoride ions, but strict threefold symmetry would be absent. We should note that the Mössbauer results provide an additional argument against the Ca(1) site, since the theoretically calculated antimony nuclear quadrupole-coupling constant for Sb^{3+}

replacing Ca(1) with no other lattice distortion is much smaller than the measured value.

The ^{19}F MAS-NMR results do not explicitly rule out the Ca(1) site as a substitution site for antimony atoms. If either of these charge-compensation schemes above were invoked, peak *B* in the ^{19}F MAS-NMR spectra would have to be assigned to a fluoride ion in the column of fluorides containing the vacancy (or oxygen ion), and peak *A* would be assigned to two identical fluoride ions in the other two chains of the triangular prism. This model offers no explanation for the greater linewidth of peak *A* compared to peak *C* (Table I). Finally, the presence of only one fluoride ion corresponding to peak *B*, rather than two essentially equivalent fluoride ions above and below the vacancy, is difficult to rationalize in the above model. Perhaps the most definitive experiment to rule out this model solely on the basis of ^{19}F MAS-NMR would be to demonstrate with a type of REDOR experiment¹⁹ that peak *A* arises from two adjacent fluoride ions in the same chain.

The ^{31}P MAS-NMR results provide the strongest evidence against the Ca(1) site. This conclusion is based on the lack of a distinct antimony-related resonance in the ^{31}P MAS-NMR spectra, despite the expectation that such a peak should be readily observable (see above).

2. Ca(2) site

The combined MAS-NMR results seem to rule out this possibility. As discussed in Sec. IVC 1, an antimony atom occupying a Ca(2) site would be expected to produce a detectable additional peak in the ^{31}P MAS-NMR spectra, which is not observed.

The ^{19}F MAS-NMR results provide additional evidence against the Ca(2) site. If an antimony atom were in the Ca(2) site, a fluoride ion adjacent to the antimony atom would be replaced by an O^{2-} ion for charge compensation. Assuming that the two fluoride ions adjacent to the O^{2-} ion were responsible for peak *A*, the spin-diffusion results require that the fluoride nucleus giving rise to peak *B* must be in an adjacent fluoride chain (Fig. 9). However, this fluoride nucleus would be distant (700 pm away) from the antimony atom and separated from it by five chemical bonds (Sb-O-P-O-Ca-F); the perturbation of the fluorine chemical shift observed for peak *B* is more difficult to rationalize in this case than for the phosphate model below.

3. Phosphate site

Both the ^{31}P and ^{19}F MAS-NMR results support the phosphate site as the location of antimony in the apatite lattice. If an antimonate tetrahedron (three oxygen atoms and a lone electron pair surrounding antimony) occupied the site of a phosphate tetrahedron and the lone electron pair on the antimony atom occupied the site of an oxygen atom nearest the fluoride chain (Fig. 12), the environment of two Ca(2) ions normally bonded to this oxygen atom would be perturbed. The two fluoride ions adjacent to each of these perturbed Ca(2) ions can therefore be assigned to peak *A*. Since these two fluoride ions do not have an identical bonding geometry to the an-

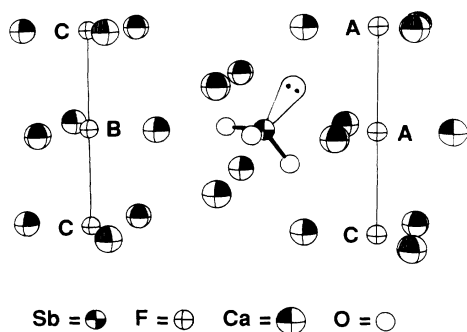


FIG. 12. ORTEP drawing of fluorapatite lattice, with antimony(III) and its lone pair placed exactly at the phosphate site. The assignment of fluoride ions to peaks *A* and *B* in the ^{19}F MAS-NMR spectra is indicated (see text).

timony ion, they would be expected to have slightly different chemical shifts. Such a small chemical-shift difference may be responsible for the approximately 120 Hz (0.32 ppm) greater linewidth of peak *A* compared to peak *C*. The downfield shift of peak *A* may be qualitatively ascribed to an increased paramagnetic contribution in the Ramsey theory of chemical shifts,⁶⁰ as a result of a greater tendency of the Ca^{+2} ion missing an O^{2-} ligand to withdraw electrons from the fluoride ions. To satisfy the spin-diffusion results (Fig. 9), peak *B* must be assigned to a fluoride ion in the closest linear chain of fluoride ions, with a three-bond bonding network of Sb-O-Ca-F linking the antimony ion to the fluoride ion (Fig. 12). The chemical-shift difference between peaks *B* and *C* (1.6 ppm) is expected to be less than that between peaks *A* and *C*, since the perturbation is less. Although one of the fluoride ions adjacent to the peak *A* fluoride ions has the same bonding network to the antimony atom (Sb-O-Ca-F) as the fluoride ion assigned to peak *B*, we must assume that its chemical shift is undetectably different from that of the peak *C* fluoride ions.

The lack of an antimony-related peak in the ^{31}P MAS-NMR spectra is also readily explicable if antimony occupies the phosphate site. The bonding network to the nearest phosphorus atom would be Sb-O-Ca-O-P. The presence of four bonds between the antimony and phosphorus atoms, rather than two bonds as for the Ca(1)- and Ca(2)-site models, would plausibly result in the absence of a significant perturbation of the ^{31}P chemical shift.

Having shown that peaks *A* and *B* arise from fluorine nuclei near an antimony atom with a distinct orientation in the phosphate site, we will now attempt to assign the 73.1-ppm peak. As shown in Sec. IV A, the fluorine nuclei giving rise to the weak peak at 73.1 ppm must be in the fluorapatite lattice. The peak at 73.1 ppm does not arise from fluoride ions at the surface of the crystallites, since the specific-surface-area measurements indicate that only approximately $1/10^6$ of the fluoride ions are at or near the surface of the crystallites, whereas the intensity of the 73.1-ppm peak is as high as 4.6% of the total intensity. The 73.1-ppm peak in the ^{19}F MAS-NMR spectra of the fluorapatite samples containing 2.1, 1.7, and 1.3

wt % antimony cannot be due to the antimony atom in the phosphate site that gives rise to peaks *A* and *B*, since its intensity does not correlate with that of these latter peaks. The 73.1-ppm peak is not due to an antimony atom that occupies one of the Ca sites, based on the ^{31}P NMR arguments in Secs. IV C 1 and IV C 2.

It is possible that the 73.1-ppm peak arises from an apatitic fluoride ion near an antimony atom in the phosphate site whose electron lone pair occupies the site of a missing oxygen atom directed away from the nearest adjacent fluoride chain (unlike the antimony associated with *A* and *B*). Supporting this assignment is the correlation observed (except for the 3.0-wt % sample) of the intensity of the 73.1-ppm peak with the amount of antimony *not* associated with peaks *A* and *B*. Specifically, when the ^{19}F MAS-NMR intensity of the 73.1-ppm peak (expressed as the fraction of the total intensity) is plotted versus the mole fraction of antimony atoms in the sample not associated with peaks *A* and *B*, the three points can be fit to a line with a slope of 1.01 and a correlation coefficient of 0.93, indicating that there is one antimony atom associated with each fluorine atom giving rise to the 73.1-ppm peak. The increased linewidth of this peak may be due to an observable quadrupolar effect from the antimony nuclei. One fact is not convincingly rationalized by the assignment of the 73.1-ppm peak to a single fluorine nucleus perturbed by an antimony atom in the phosphate-substitution site with a different Sb lone-pair orientation. The chemical-shift difference between the 73.1-ppm peak and the main peak at 64.0 ppm is twice as large as that between *A* and the main peak, even though the distance and bonding linkage from the antimony atom to the nearest fluorine nuclei are nearly the same for the proposed assignments.

V. CONCLUSIONS

We have shown by ^{31}P and ^{19}F MAS-NMR of antimony-doped fluorapatite samples that antimony(III) occupies the phosphate site in the apatite lattice rather than one of the cationic (calcium) sites. Our data strongly support the model of Mishra *et al.*,⁵ in which the PO_4^{3-} group is replaced by a (slightly displaced) SbO_3^{3-} moiety, with the antimony 5s-electron lone pair directed toward the missing oxygen-atom site. The MAS-NMR results also show that these samples contain a maximum of 1.6 wt % Sb^{3+} in this well-defined lattice site, with most of the excess antimony going into a secondary site and/or secondary phase.

Because of the paucity of other studies of antimony(III) dopant sites in ionic lattices, it is difficult to draw conclusions regarding the generality of the behavior we observe. At least in this one instance, we have shown that Sb^{3+} , rather than substituting for a divalent cation of larger ionic radius (99 pm vs 76 pm),⁵⁸ instead essentially replaces a formal $\text{P}^{5+}\text{-O}^{2-}$ moiety. In this sense antimony(III) could be said to resemble a nonmetal more than an alkaline-earth ion. The oxygen coordination polyhedra may also be influential in determining the bonding mode, with the three oxygen atoms of a phosphate group providing the hemihedral coordination common in crystal structures of antimony(III) compounds.

High-field ^{19}F MAS-NMR is a useful technique for

quantifying the amount of antimony actually incorporated into the fluorapatite lattice. It can readily detect antimony levels as low as 0.2 wt % in a single scan. This study demonstrates several advantages to studying substitution by dopants through their effect on magnetically active nuclei rather than by direct observation of the dopant nuclear resonance, even assuming the latter is observable. First, it is easier to distinguish actual incorporation of the dopant into the host lattice from possible formation of secondary phases. Also, a single dopant site may result in unequal perturbations of a number of atoms of the host, thus providing more detailed structural information. The influence of spin diffusion upon the ¹⁹F MAS-NMR spin-lattice relaxation times was important in this study in establishing that the perturbed peaks arise from fluoride ions in the apatitic lattice. We have shown that the rate of spin diffusion between spectrally resolved peaks can be quantitatively measured using the selective-excitation SPARTAN pulse sequence in a one-dimensional NMR experiment. The spectral spin-diffusion rates measured using the SPARTAN sequence have enabled us to assign the two peaks perturbed by antimony to fluoride ions on *different* linear chains. Difference spectra have shown that these two peaks are present in a 2:1 intensity ratio, consistent with expectations based on molecular models.

The observation of spectral spin diffusion for MAS spinning speeds greater than the maximum dipolar coupling in the spin network is an interesting experimental fact; we are aware of only one other comparable result that has been briefly alluded to.⁶¹ If this behavior is fairly general (occurring either via level crossing or atomic motion), spin-diffusion measurements obtained by using the SPARTAN sequence may prove very useful for assigning MAS-NMR peaks. It would also be worthwhile to investigate theoretically as well as experimentally the "quenching" of spin diffusion by MAS at high spinning speeds.^{28,42}

ACKNOWLEDGMENTS

We are grateful to Dr. Chung-Nin Chau for providing the samples of strontium, strontium-calcium, barium fluorapatite, and antimony phosphate, to Dr. Barry DeBoer for sample characterization by x-ray powder diffraction, and to Dr. Ernest Dale for kindly providing results for the antimony-doped fluorapatite samples, as well as for useful comments and discussions. We thank Dr. Sam Kaplan for suggesting the selective spin-diffusion experiment. We gratefully acknowledge GTE Electrical Products Corporation for partial financial support of this work.

*Author to whom correspondence should be addressed. Present address: Code 6120, Naval Research Laboratory, Washington, D.C. 20375-5000.

¹S. Naray-Szabo, *Z. Kristallogr.* **75**, 387 (1930).

²D. McConnell, in *Applied Mineralogy*, edited by A. V. D. Frechette, H. Kirsch, L. B. Sand, and F. Trojer (Springer-Verlag, New York, 1973).

³R. W. Warren, *Phys. Rev. B* **2**, 4383 (1970).

⁴R. W. Warren and R. Mazelsky, *Phys. Rev. B* **10**, 19 (1974).

⁵K. C. Mishra, R. J. Patton, E. A. Dale, and T. P. Das, *Phys. Rev. B* **35**, 1512 (1987).

⁶T. S. Davis, E. R. Kreidler, J. A. Parodi, and T. F. Soules, *J. Lumin.* **4**, 48 (1971).

⁷R. W. Warren, F. M. Ryan, R. H. Hopkins, and J. Van Broekhoven, *J. Electrochem. Soc.* **122**, 752 (1975).

⁸B. G. DeBoer, A. Sakthivel, J. R. Cagle, and R. A. Young, *Acta Crystallogr. B* **47**, 683 (1991).

⁹J. G. Rabatin, G. R. Gillooly, and J. W. Hunter, *J. Electrochem. Soc.* **114**, 956 (1967).

¹⁰E. R. Andrew, in *Progress in Nuclear Magnetic Resonance Spectroscopy*, edited by J. W. Emsley, J. Feeney, and L. H. Sutcliffe (Pergamon, New York, 1971).

¹¹W. P. Rothwell, J. S. Waugh, and J. P. Yesinowski, *J. Am. Chem. Soc.* **102**, 2637 (1980).

¹²J. P. Yesinowski and M. J. Mobley, *J. Am. Chem. Soc.* **105**, 6191 (1983).

¹³K. A. Smith and D. P. Burum, *J. Magn. Reson.* **84**, 85 (1989).

¹⁴M. Mehring, in *NMR Basic Principles and Progress*, edited by P. Diehl, E. Fluck, and R. Kosfeld (Springer-Verlag, Berlin, 1976), Vol. 11.

¹⁵B. C. Gerstein, C. Chow, R. G. Pembleton, and R. C. Wilson, *J. Phys. Chem.* **81**, 565 (1977).

¹⁶J. P. Yesinowski and H. Eckert, *J. Am. Chem. Soc.* **109**, 6274 (1987).

¹⁷J. P. Yesinowski, H. Eckert, and G. R. Rossman, *J. Am. Chem. Soc.* **110**, 1376 (1988).

¹⁸M. M. Maricq and J. S. Waugh, *J. Phys. Chem.* **70**, 3300 (1979).

¹⁹T. Gullion and J. Schaefer, *J. Magn. Reson.* **81**, 196 (1989).

²⁰M. Munowitz, W. P. Aue, and R. G. Griffin, *J. Chem. Phys.* **77**, 1686 (1982).

²¹J. E. Roberts *et al.*, *J. Am. Chem. Soc.* **109**, 4163 (1987).

²²C. E. Bronnimann, R. C. Zeigler, and G. E. Maciel, *J. Am. Chem. Soc.* **110**, 2023 (1988).

²³P. Caravatti, J. A. Deli, G. Bodenhausen, and R. R. Ernst, *J. Am. Chem. Soc.* **104**, 5506 (1982).

²⁴A. Kubo and C. A. McDowell, *J. Chem. Phys.* **89**, 63 (1988).

²⁵V. Bork and J. Schaefer, *J. Magn. Reson.* **81**, 196 (1989).

²⁶L. B. Moran, J. K. Berkowitz, and J. P. Yesinowski (unpublished).

²⁷G. Bodenhausen, R. Freeman, and G. A. Morris, *J. Magn. Reson.* **23**, 171 (1976); G. A. Morris and R. Freeman, *J. Magn. Reson.* **29**, 433 (1978).

²⁸A. Kubo and Charles A. McDowell, *J. Chem. Soc. Faraday Trans.* **84**, 3713 (1988).

²⁹J. L. Carolan, *Chem. Phys. Lett.* **12**, 389 (1971).

³⁰A. M. Vakhrameev, S. P. Gabuda, and R. G. Knubovets, *J. Struct. Chem. (USSR)* **19**, 256 (1978).

³¹W. Van der Lugt and W. J. Caspers, *Physica* **30**, 1658 (1964).

³²W. P. Rothwell and J. S. Waugh, *J. Chem. Phys.* **74**, 2721 (1981).

³³A. T. Kreinbrink *et al.*, *J. Magn. Reson.* **88**, 267 (1990).

³⁴C. Connor, A. Naito, K. Takegoshi, and C. A. McDowell, *Chem. Phys. Lett.* **113**, 123 (1984).

- ³⁵N. Bloembergen, *Physica* **15**, 386 (1949).
- ³⁶A. Abragam, *The Principles of Nuclear Magnetism* (Oxford University Press, London, 1961), Chaps. V and IX.
- ³⁷D. Suter and R. R. Ernst, *Phys. Rev. B* **25**, 6038 (1982).
- ³⁸E. R. Andrew, A. Bradbury, R. G. Eades, and T. Wynn, *Phys. Lett.* **4**, 99 (1963).
- ³⁹P. Caravatti, M. H. Levitt, and R. R. Ernst, *J. Magn. Reson.* **68**, 323 (1986).
- ⁴⁰D. L. Vanderhart, *J. Magn. Reson.* **72**, 13 (1987).
- ⁴¹C. A. Fyfe, H. Gies, and Y. Feng, *J. Am. Chem. Soc.* **111**, 7702 (1989).
- ⁴²D. Suter and R. R. Ernst, *Phys. Rev. B* **32**, 5068 (1985).
- ⁴³P. M. Hendrichs, M. Linder, and J. M. Hewitt, *J. Chem. Phys.* **85**, 7077 (1986).
- ⁴⁴P. Robyr, B. H. Meier, and R. R. Ernst, *Chem. Phys. Lett.* **162**, 417 (1989).
- ⁴⁵M. G. Colombo, B. H. Meier, and R. R. Ernst, *Chem. Phys. Lett.* **146**, 189 (1988).
- ⁴⁶D. P. Raleigh, M. H. Levitt, and R. G. Griffin, *Chem. Phys. Lett.* **146**, 71 (1988).
- ⁴⁷J. Kowalewski, *Progress In NMR Spectroscopy*, edited by J. W. Emsley, J. Feeney, and L. H. Sutcliffe (Pergamon, Oxford, 1976), Vol. 11, pp. 1–74.
- ⁴⁸K. Hirao, H. Nakatsuji, and H. Kato, *J. Am. Chem. Soc.* **95**, 31 (1973).
- ⁴⁹R. Eckman, *J. Chem. Phys.* **79**, 524 (1983).
- ⁵⁰D. P. Raleigh, E. T. Olejniczak, and R. G. Griffin, *J. Chem. Phys.* **89**, 1333 (1988).
- ⁵¹E. T. Olejniczak, S. Vega, and R. G. Griffin, *J. Chem. Phys.* **81**, 4804 (1984).
- ⁵²J. Herzfeld and A. E. Berger, *J. Chem. Phys.* **73**, 6021 (1980).
- ⁵³N. Zumbulyadis, P. M. Hendrichs, and R. H. Young, *J. Chem. Phys.* **74**, 1603 (1981).
- ⁵⁴J. Bohm, D. Fenzke, and H. Pfeifer, *J. Magn. Reson.* **55**, 197 (1983).
- ⁵⁵W. W. Fleming *et al.*, *Macromolecules*. **13**, 460 (1980); E. M. Menger and W. S. Veeman, *J. Magn. Reson.* **46**, 257 (1982).
- ⁵⁶E. Dale (private communication).
- ⁵⁷G. L. Turner, K. A. Smith, R. J. Kirkpatrick, and E. Oldfield, *J. Magn. Reson.* **70**, 408 (1986).
- ⁵⁸*Handbook of Chemistry and Physics*, 57th ed., edited by R. C. Weast (CRC, Cleveland, 1976).
- ⁵⁹B. Kinberger, *Acta Chem. Scand.* **24**, 320 (1970).
- ⁶⁰N. F. Ramsey, *Phys. Rev.* **78**, 699 (1950).
- ⁶¹N. J. Clayden, *J. Magn. Reson.* **68**, 360 (1983).

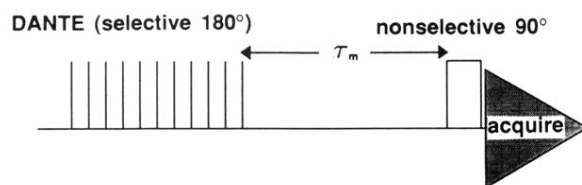


FIG. 2. SPARTAN pulse sequence for measuring spectral spin diffusion (see text).